Available online at www.sciencedirect.com
ScienceDirect
Engineering Structures 29 (2007) 431–439
ENGINEERING STRUCTURES
www.elsevier.com/locate/engstruct

Limit analysis of reinforced masonry vaults

P. Roca*, F. López-Almansa, J. Miquel, A. Hanganu

Universitat Politècnica de Catalunya, Jordi Girona 1-3, 08034 Barcelona, Spain

Received 6 October 2005; received in revised form 13 March 2006; accepted 10 May 2006
Available online 7 July 2006

Abstract

Reinforced brick masonry has experienced only scarce use as a fully structural material due to, among other reasons, the lack of design criteria and calculation tools allowing a scientific, but also practical, engineering approach to design and assessment. Aiming at contributing to a more widespread use of this material, a simplified method for the ultimate analysis of reinforced masonry arches and cylindrical vaults, based on the lower-bound theorem (or static approach) of plasticity, has been developed. This approach has been satisfactorily validated by comparison with experimental and numerical results obtained by more accurate numerical models.

Keywords: Reinforced masonry; Masonry vaults; Limit analysis; Static approach

1. Introduction

Reinforced masonry, consisting of a combination of plane inlaid bricks and continuous mortar joints with embedded steel reinforcement, has demonstrated important architectural and structural possibilities mainly through the realizations of the Uruguayan engineer Eladio Dieste [1,2]. Among other interesting buildings, Dieste designed and constructed appealing simple or double curvature single-leaf, long-span reinforced masonry shells such as in the Church of Altantida or the Caputto Warehouse in Montevideo, Uruguay, the latter spanning up to 46.5 m.

Reinforced masonry construction is not only interesting because of its structural and architectural possibilities; brick masonry is inexpensive and available everywhere, while it offers interesting qualities in terms of aesthetics, thermal insulation, small maintenance costs and sustainability. However, reinforced masonry shells have not experienced much significant use or interest, beyond Dieste's work. This is due to reasons related with, first, the amount of handwork required and, second, the lack of objective, scientifically-based available design criteria and simulation tools.

On the one hand, a significant amount of handwork may be necessary if traditional construction procedures, based on personnel skills and non-industrial forming solutions, are used. However, handwork can be reduced to a minimum by means of industrialized construction procedures such as those proposed by the Craft EC project ISOBRICK oriented to the design and construction of cylindrical short- to medium-span reinforced masonry roofs [3]. The process is based on a semi-prefabricated construction in which flexible meshes, including the bricks and part of the reinforcement, are previously manufactured to be later installed and shaped in the site according to the desired vaulted geometry; mortar or concrete are then poured to fill the joints and to create a continuous topping (Fig. 1).

On the other hand, Dieste's structural designs relied mostly on his vast experience and refined personal understanding. Modern designers may feel more compelled to use an objective approach involving specific design criteria and calculation methods adequately validated by experimental evidence. As a necessary complement to the proposed construction technology, the ISOBRICK project also contributed with experimental research on the strength performance of short- and medium-span cylindrical shells (see in Section 4.1). In turn, the experimental results allowed the validation of a numerical method (termed PRO-SHELL) for the analysis of reinforced masonry shells based on the theory of continuum damage (see in Section 4.2). The capacity of this method to produce a detailed simulation of the service and ultimate response of reinforced masonry shell structures has been proven satisfactorily. However, the use of this method requires

* Corresponding author.
E-mail address: pere.roca.fabregat@upc.edu (P. Roca).

0141-0296/$ - see front matter © 2006 Elsevier Ltd. All rights reserved.
doi:10.1016/j.engstruct.2006.05.009

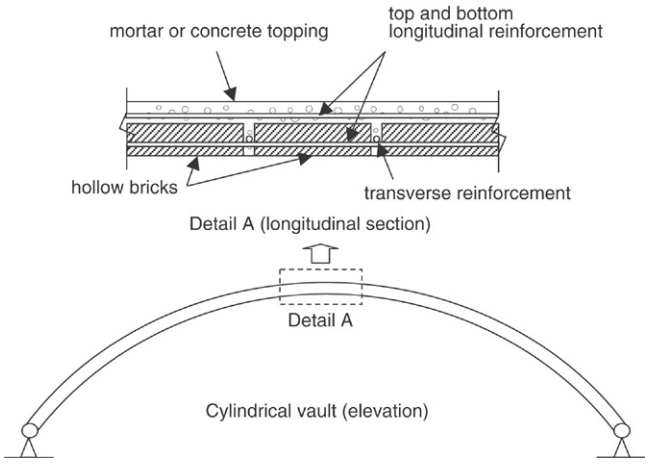

Fig. 1. Industrialized reinforced masonry construction technology [3].

significant computer effort and advanced structural and numerical knowledge. A simpler tool for analysis, usable for the practical design and assessment of masonry shells, is also needed.

This paper presents a simplified tool (termed DBS-ROOF) for the analysis of cylindrical short- and medium-span reinforced masonry shells. The aim at developing DBS-ROOF was to provide an easy to use, interactive and user-friendly tool useful to practical potential users (designer architects, engineers and construction companies) for guiding the design process and assessing the structural viability and safety of the resulting vaults. The tool can also be applied to the ultimate analysis of reinforced concrete or plain masonry or concrete arches. The method stems from the application of plastic analysis to the assessment of unreinforced stone or brick masonry arches and, in essence, preserves the simplicity and operation of this well-known approach. Because of its geometrical character, the method can be easily and interactively operated by means of an adequate graphic user interface. This calculation tool has been validated by comparison with experimental and numerical results obtained within the ISOBRICK project.

2. Theoretical background

The application of plastic analysis to the assessment of unreinforced masonry arches is today well acknowledged thanks to the contribution of Heyman [4,5]. Within the static approach, limit analysis involves, as a first step, the determination of a thrust line in equilibrium with the external loads. The thrust line is defined as the locus of the points of application of the sectional forces throughout the arch. Where the thrust line becomes tangent to the boundaries of the arch, meaning that the only possible contact between sections or blocks is reduced to a point or to a very reduced portion of the section yielded in compression, rotation becomes possible and a hinge is formed. According to the safe (or lower-bound) theorem, if it is possible to find a thrust line in equilibrium with the applied loads and fitting within its boundaries, then the structure is safe (Fig. 2). According to the uniqueness theorem, if it is possible to find a thrust line in equilibrium with the applied loads and fitting within its boundaries, which causes a collapsing mechanism, then the loads are the true ultimate ones and the mechanism is the true ultimate one (Fig. 2). Such a mechanism will be produced by the generation of a number of hinges, each one, in turn, being caused by the thrust line becoming tangent to the boundaries of the arch.

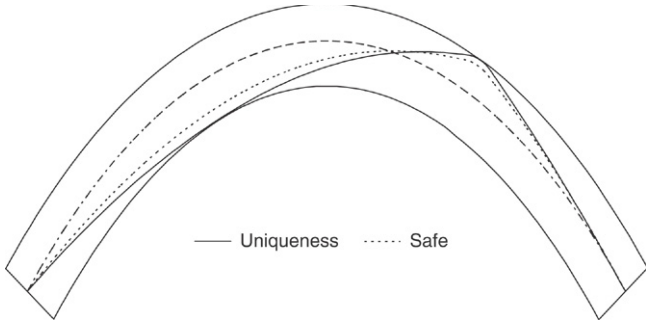

Fig. 2. Example of thrust lines corresponding to a concentrated load for the safe and the uniqueness theorems.

Experiments carried out on reinforced masonry cylindrical vaults (Section 4.1) have shown that the ultimate response of such structures is governed by the development of ductile collapse mechanisms caused by the generation of a certain number of plastic hinges. In fact, the failure modes are qualitatively similar to those experienced by unreinforced brick or masonry arches. Furthermore, all the tested reinforced masonry structures exhibited an important ductility, i.e., a significant capacity to accept deformation until collapse. This ductility was observed even in the case of structures with a very small amount of reinforcement. In fact, since the structures are arranged in the shape of an arch, the capacity to fully develop ductile collapsing mechanisms is theoretically certain even if no reinforcement exists. The possibility of applying both the static or the kinematic approach to the analytical calculation of reinforced masonry cylindrical shells has been already explored by Lourenço et al. [6].

3. Proposed method for the analysis of reinforced cylindrical shells

3.1. Description of geometry and support conditions

The method proposed herein consists of a numerical technique applicable to the ultimate analysis of arbitrarily shaped arches or cylindrical shells. The method is based on limit analysis and uses the static approach (the aforementioned safe – or lower-bound – and uniqueness theorems) to determine the ultimate capacity of the structures analyzed by means of an optimization process.

For that purpose, the geometry is described by decomposing the entire arch in a series of equally spaced short segments (or fictitious "voussoirs") limited by sections oriented perpendicularly to the axis (Fig. 3). This procedure affords the description of the geometry and the equilibrium condition of any type of arch or elementary voussoir. In particular, voussoirs with variable thickness or width are also acceptable.

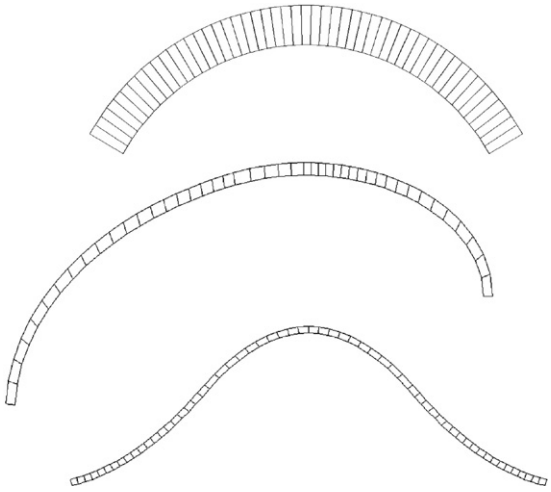

Fig. 3. Examples of curved members decomposed into fictitious voussoirs.

The adequate modeling of the support conditions at the springings of the arches or vaults is of great importance to determine realistic thrust line solutions. The following alternative support conditions are considered (Fig. 4): (a) perfectly hinged ends, in which case the thrust line is set to coincide with the position of the axis of physical hinges materialized at the springings; (b) simple supports offering direct contact spreading totally or partially on the surface of the springing; (c) perfectly clamped ends, where the thrust line is allowed to move freely between top and bottom strength boundaries defined in Section 3.2; and (d) partially clamped ends, in which case the thrust line is set to vary within a restricted region contained within the boundaries. Condition (1) requires a specific device able to work as a true hinge. Conditions (c) and (d) require specific reinforcement details affording the transmission of the end bending moments; in fact, a perfectly clamped end, with no rotation allowed at the end, seems difficult to obtain using conventional reinforcing details; the consideration of a partially clamped support seems more reasonable where a clamped end is formed by doweling steel bars (Fig. 4(d)). In Fig. 4, the limit thrust lines are those with maximum acceptable eccentricity at the support.

3.2. Modeling of reinforced masonry vaults

The method can be easily extended to describe the mechanical effect of steel reinforcement in a geometrical way. The reinforcement is modeled as an increase of the depth of the arch described by means of equivalent top and bottom boundaries, or *strength boundaries*, to be considered for the application of the plastic theorems. The strength top or bottom boundaries are defined as the maximum (or top) and minimum (or bottom) eccentricities of applied forces accepted by the reinforced section.

The position of the strength boundaries depends on the amount of reinforcement, the concrete cover and the compressive strength of concrete. The distance between the strength boundaries and the axis of the arch can be determined by assuming a certain distribution of stresses and forces in the section at the ultimate condition.

According to Eurocode 6 [7], the distribution of stresses in reinforced masonry sections experiencing a ultimate condition

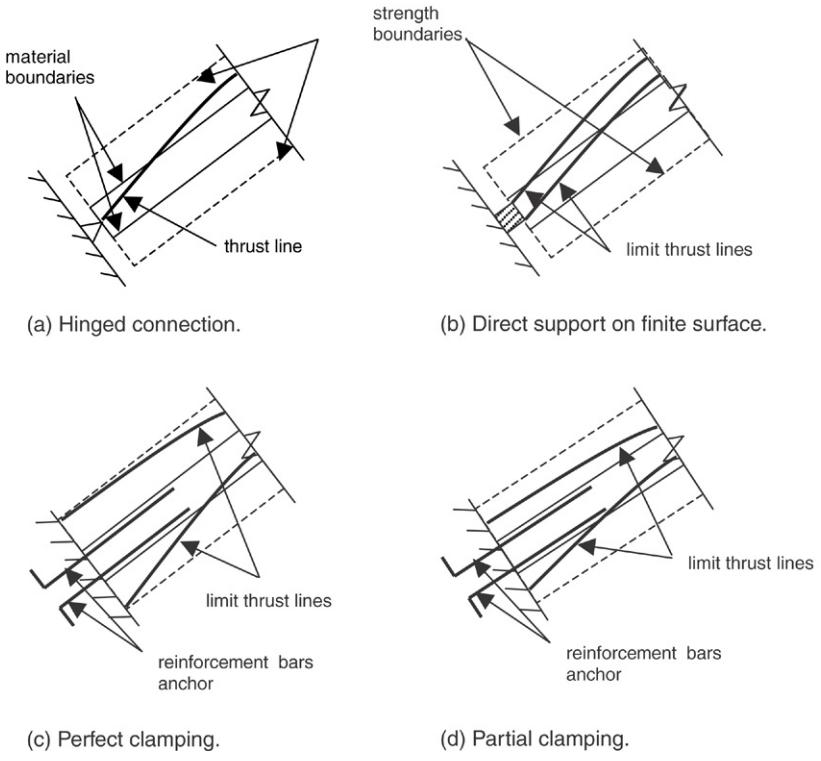

Fig. 4. Different support conditions: (a) hinged; (b) direct support; (c) perfect clamping; (d) partial clamping.

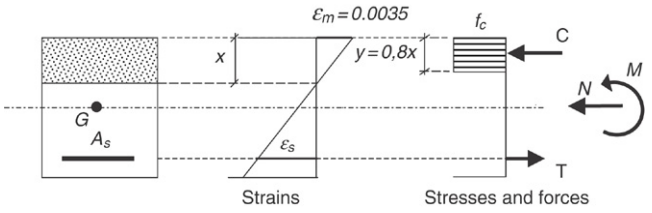

Fig. 5. Simplified rectangular distribution of stresses at the ultimate condition.

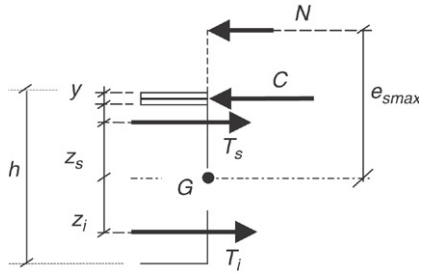

Fig. 6. Assumed distribution of stresses and forces at failure.

in bending or compression can be modeled by means of a parabolic diagram or, in a more simplified way, by the rectangular diagram of Fig. 5, where G is the centroid of the section, N is the axial force applied to the section, M is the ultimate moment, C is the force resisted by the compressed material, T is the force experienced by the reinforcement, y is the depth of the compressed block, ε_m, set equal to 0.0035, is the ultimate unit strain of the compressed material (masonry or concrete) and A_s is the section of steel reinforcement in tension. The stresses in the compressed block are assumed uniform and equal to the uniaxial compression strength f_c. The steel is assumed to behave according to a perfect elastoplastic bilinear diagram with a horizontal second branch defined by the yield stress ε_y.

The diagram of Fig. 5 can be easily adapted to the distribution of reinforcement and forces existing in a reinforced masonry vault such as the one described in Fig. 1. In this case, two different layers of steel, distributed as indicated in Fig. 6, are considered.

Depending on the depth of the compressed block, the steel closest to the maximum compressed fibre will work in compression or in tension, producing either a positive or a negative T_s force. Furthermore, both the top and the bottom reinforcement can work in elastic or plastic condition. As shown by the experiments, for conventional topping mortar or brick strengths, and for the usual covers (between 1 and 3 cm), the depth of the neutral axis is small enough as to cause tensile forces to both the lower and the upper reinforcement. However, the use of poor mortars, with low compression strength, may cause the upper reinforcement to work in compression.

The equations providing the ultimate moment can be derived from the compatibility and the equilibrium conditions and the adopted stress–strain relationships. The procedure to solve the equations is the same one used in the conventional calculation of reinforced concrete and is not reproduced here.

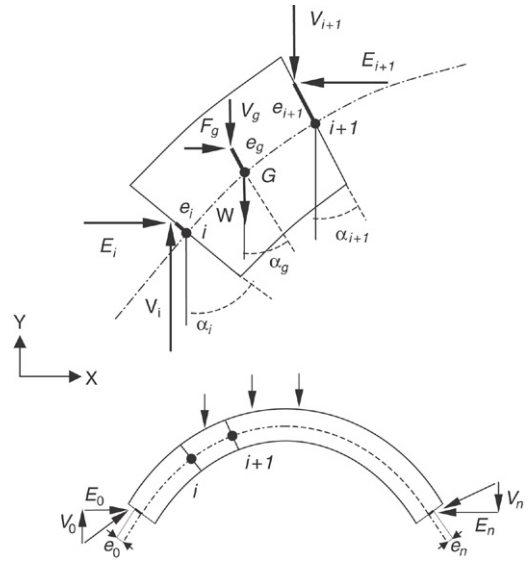

Fig. 7. Forces acting on the arch (below) and the elementary voussoir (above).

Once the ultimate moment is known, the value of a maximum possible eccentricity $e_{s\max}$ results from

$$e_{s\max} = \frac{M}{N}. \tag{1}$$

By applying Eq. (1) to both the ultimate positive and negative moments resisted by the section, the maximum top and bottom eccentricities, e_{top} and e_{bot}, determining the strength boundaries, can be calculated.

3.3. Generation of a thrust line solution

Overall equilibrium of the arch provides three equations (vertical forces, horizontal forces and moments) to relate the unknowns, namely the vertical and horizontal reactions at the left and right supports, V_0, E_0, V_n, and E_n, and the corresponding points of application at the end sections, defined by the eccentricities with respect to the axis of the arch, e_0 and e_n, (Fig. 7). Equilibrium does not determine a single solution, but just a range of solutions constrained by the three equilibrium equations. In the present method, E_0, e_0, and e_n are chosen as the variables or degrees of freedom determining each possible solution. Once the reactions are known for a certain triplet (E_0, e_0, e_n), internal equilibrium can be considered to generate the corresponding thrust line.

Thrust line solutions in equilibrium with the external loads are generated by subsequently balancing all the loads acting at each individual voussoir (see Fig. 7). Let i and $i + 1$ be the centroids of the end sections and let G be the centroid of the entire voussoir. The loads applied on the voussoir include the vertical and horizontal forces acting at the end sections, V_i, E_i, V_{i+1}, and E_{i+1}; the self-weight of the voussoir, W; and possible external vertical and horizontal concentrated loads acting at the section of the centroid, V_g, F_g. e_i, e_{i+1} are the eccentricities of the forces at the end sections and e_g is the eccentricity of the external forces V_g, F_g.

The equilibrium of vertical forces, horizontal forces and moment (Fig. 7) leads to the following expressions:

$$E_{i+1} = E_i + F_g \tag{2}$$

$$V_{i+1} = V_i - W - V_g \tag{3}$$

$$\begin{aligned} &E_i(y_i + e_i\cos\alpha_i) - V_i(x_i - e_i\sin\alpha_i) + Wx_g \\ &\quad + F_g(y_g + e_g\cos\alpha_g) + V_g(x_g - e_g\sin\alpha_g) \\ &= E_{i+1}(y_{i+1} + e_{i+1}\cos\alpha_{i+1}) \\ &\quad - V_{i+1}(x_{i+1} - e_{i+1}\sin\alpha_{i+1}) \end{aligned} \tag{4}$$

where (x_i, y_i), (x_{i+1}, y_{i+1}), (x_g, y_g) are the coordinates of points i, $i+1$ and G.

The above equation permits the determination of e_{i+1} once the value of e_i is already known from the study of the previous contiguous voussoirs. The set of eccentricities $\{e_1, e_2, \ldots, e_n\}$ determine the shape of the thrust line across all sections between voussoirs. Thus, the thrust line is obtained as a polygonal approach whose accuracy will depend on the density of the decomposition. As observed from the analyses carried out, a short number of voussoirs is enough to obtain satisfactory results. Calculations undertaken for a typical catenary vault (example V1 of Section 4.1) showed that the error in the ultimate load was of 27%, 9.1%, 2%, 1% and 0% for calculations carried out with 5, 10, 20, 30 and 40 voussoirs respectively. All the examples presented later in this paper have been modeled with 40 voussoirs.

Note that the strength boundaries $e_{\text{top}}, e_{\text{bot}}$ are dependent with the value of the axial force N acting at each section of the arch. Because of that, the resulting boundaries show an expectable, theoretically consistent but brusque variation where vertical concentrated forces are applied (Fig. 8(a)). For the same reason, the strength boundaries must be recalculated for each different applied loading. Because of this effect, three different alternative ways to represent graphically the solutions are envisaged. As a first possibility, the *true thrust line* mode is considered, in which the already defined strength boundaries and the thrust line are represented (Fig. 8(a)). The second possibility (*moment ratio* mode) consists of representing the curves which result from multiplying the eccentricities by the axial forces experienced by each section; in that case, the graphic represents the moment acting on the section compared with the maximum acceptable moments (Fig. 8(b)). The third possibility (*normal* mode) consists on normalizing the strength boundaries along the arch, so that they become constant, and then scaling the eccentricity of the thrust line accordingly. As a consequence, the equivalent boundary lines do not depend on the applied loads. Although the real meaning of the lines is lost, this graphical mode is advantageous because it allows the direct comparison of lines corresponding to different loading hypotheses with respect to constant equivalent limits (Fig. 8(c)).

3.4. Application of plastic theorems

A method envisaged by Andreu et al. [8] is used to determine the thrust line solutions satisfying either the safe theorem or the uniqueness theorem. For that purpose, a thrust line is described by a vector defined as

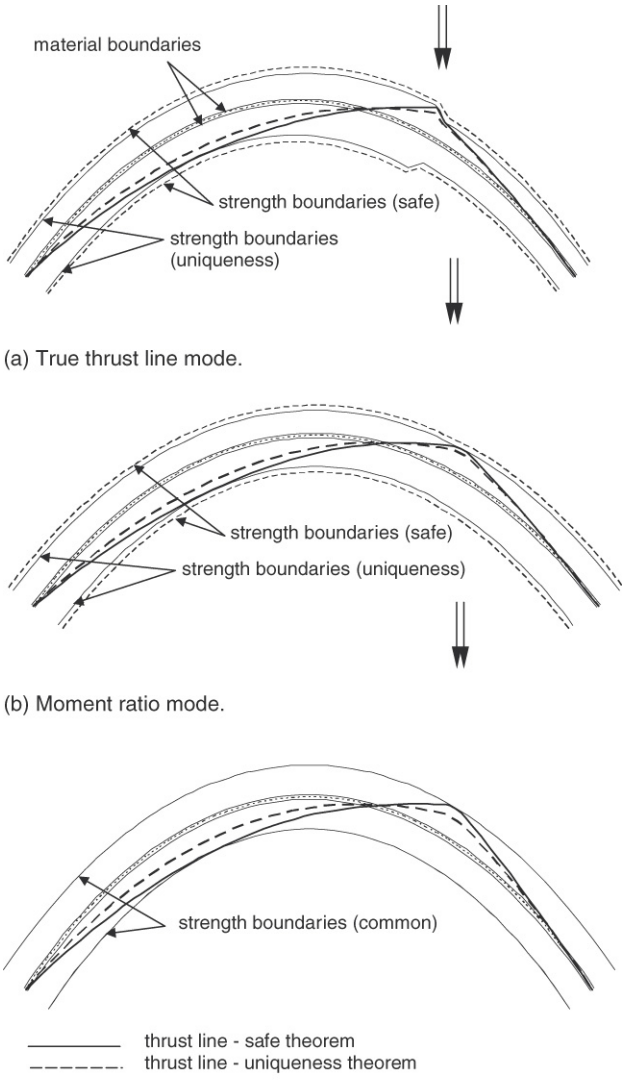

Fig. 8. Different modes of representing a thrust line solution. The examples correspond to solutions verifying the safe and the uniqueness theorems.

$$\boldsymbol{X} = \{e_0, e_1, \ldots, e_{n-1}, e_n\}^T \tag{5}$$

where e_0 and e_n are the eccentricities of the thrust line solution at the end sections of the arch, and $e_1, e_2, \ldots, e_{n-1}$ are the eccentricities at the sections limiting the consecutive voussoirs, n being the number of voussoirs.

Because of the equilibrium constraint, and for a given set of external loads, $\boldsymbol{X}$ is in fact a function of the eccentricities and horizontal reaction, chosen as the free variables as mentioned in Section 3.3

$$\boldsymbol{X} = \boldsymbol{X}(e_0, e_n, E_0). \tag{6}$$

The top and bottom strength boundaries are defined in a similar way as

$$\boldsymbol{E}_{\text{top}} = \{e_{\text{top},0}, e_{\text{top},1}, \ldots, e_{\text{top},n-1}, e_{\text{top},n}\}^T \tag{7}$$

$$\boldsymbol{E}_{\text{bot}} = \{e_{\text{bot},0}, e_{\text{bot},1}, \ldots, e_{\text{bot},n-1}, e_{\text{bot},n}\}^T. \tag{8}$$

Functions $D_{top}(i)$ and $D_{bot}(i)$ are defined as

$$D_{top}(i) = e_{top,i} - e_i \tag{9}$$

$$D_{bot}(i) = e_i - e_{bot,i} \tag{10}$$

A cost function $D_{min}(\boldsymbol{X})$ is defined as the minimum distance from the thrust line to the strength boundaries,

$$D_{min}(\boldsymbol{X}) = \text{Min}\{D_{top}(i), D_{bot}(i), i = 0, 1, \ldots n\}. \tag{11}$$

A solution complying with the safe theorem, if existing, can be obtained as the one providing the maximum value of $D_{min}(\boldsymbol{X})$. For that purpose, an optimization process can be carried out in which the end eccentricities e_0 and e_n, together with the reaction E_0 are set as the target variables. Let $\boldsymbol{X}_{max}$ be the solution obtained by this procedure.

The solution yielded by the optimization process doesn't necessarily describe the real state of equilibrium experienced by the structure. As mentioned, it simply consists of a way to provide, whenever possible, a solution satisfying the safe theorem.

In order to apply the uniqueness theorem, some of the loads acting on the arch must be scaled by a factor φ. The theorem will permit the determination of the value of φ for which the arch reaches the ultimate mechanism. The vector $\boldsymbol{X}$ is now also a function of such a load factor,

$$\boldsymbol{X} = \boldsymbol{X}(e_0, e_n, E_0, \varphi). \tag{12}$$

For each value of φ, applying the aforementioned optimization process will produce a solution $\boldsymbol{X}_{max}$ with maximum distance to the boundaries,

$$\boldsymbol{X}_{max} = \boldsymbol{X}_{max}(\varphi). \tag{13}$$

To obtain a solution complying with the uniqueness theorem requires the determination of a set $\{e_0, e_n, E_{0,}\varphi\}$ producing the minimum possible value of $D_{min}(\boldsymbol{X}_{max})$. The solution will consist of a thrust line becoming tangent to the boundaries in the number of sections needed to generate the mechanism.

Different optimisation methods, such as the maximum descent (gradient method) and the conjugated gradient ones, can be used to carry out the mentioned optimisation procedures [8]. However, accurate solutions can also be easily obtained by scanning a large sample of thrust line solutions; such a sample can be generated by considering small increments of the involved variables $\{e_0, e_n, E_0, \varphi\}$.

4. Comparison with experimental and numerical results

4.1. Experimental results

The experimental program undertaken in the Laboratory of Technology of Structures of the Technical University of Catalonia included two series of reinforced masonry vaults, the first one consisting of 4 specimens of 4 m of span, labeled U1–U4 and tested during 2002, and the second one consisting of 11 specimens with various spans, labeled V1–V9 and tested from 2002 to 2004 [9,3]. Cases V4 and V7 are disregarded because they did not lead to failure during the experiment. Case V8 is also disregarded because it was intentionally subjected to a horizontal imposed displacement, which cannot be easily modeled using the proposed approach. Vault G1 is a virtual case for which only numerical results are available and will be described with more detail in Section 4.3.

The specimens consisted of cylindrical shells shaped roughly according to a catenary curve. The ceramic bricks were arranged to form continuous joints both in the longitudinal and the transverse directions, where the lower reinforcing bars were embedded. In addition, a layer of mortar, 3 cm thick, topped the bricks. The total depth of all vaults was of 7.5 cm, of which 4.5 corresponded to the thickness of the bricks. The reinforcement included either a single layer of steel bars placed close to the intrados (bottom reinforcement), or two layers, each placed close to a different surface (top and bottom reinforcement). Different amounts of reinforcement, as well as different mortar compression strengths were considered. The compression strength of the bricks was of 50 MPa for vaults U1–U5 and 65 MPa for the V1–V9 ones. The reinforcement was provided by means of steel bars with diameter of 6 or 8 mm and yielding stress of 400 or 500 MPa.

Table 1 summarizes the characteristics of each vault. The reinforcement ratio indicated in Table 1 is calculated as

$$\rho = \frac{\sum A_{si}(f_{yi}/500)}{bh} \tag{14}$$

where A_{si} is the section of each i-rebar, f_{yi} is the corresponding yielding stress, b is the width of the vault and h is its total depth. Table 1 refers also to the average mechanical cover of the reinforcement, obtained as:

$$c = \frac{\sum \left(c_i + \frac{\phi_i}{2}\right) A_{si} f_{yi}}{\sum A_{si} f_{yi}} \tag{15}$$

where c_i is the geometric cover (distance between the parament and the perimeter of the rebar) and ϕ_i is the diameter of each i-rebar.

All the specimens, with the exception of vault V6, were simply supported on rigid steel frames allowing the rotations but preventing any displacements at the springings. The experiments consisted of applying a vertical load at 1/4, 1/3 or 1/2 of the span and gradually increasing it, by displacement control, until failure. The load was applied by a hydraulic actuator on a steel rigid beam spanning the full width of the vault (Fig. 9).

Special reinforcing details (similar to Fig. 4(c)) were materialized in the case of vault V6, the more slender one, to restrain the rotations at the springings and to create a sort of clamped ends. However, the fact that the vault failed without causing visible damage at one of the supports suggests that it did not actually behave as a perfect clamped support, but allowed a certain rotation.

The arches failed always (except in the case of V6) due to the development of an unstable mechanism involving 3 plastic hinges for symmetric loading and 2 plastic hinges for asymmetric loading, the supports acting as two initial hinges. As shown in Fig. 10, high ductile responses were

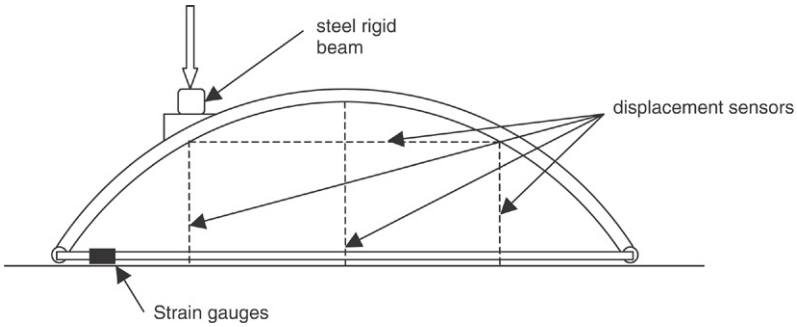

Fig. 9. Test arrangement.

Table 1
Main characteristics of vaults and loading condition

Vault	Length, rise, width (cm)	Position of loaded point	Topping/joint mortar compression strength (MPa)	Top/bottom reinforcement ratio ($\times 10^{-3}$)	Top/bottom mechanical cover (mm)
U1/U2	400, 100, 109	1/4*L*	21.0/13.0	0/3.35	–/19
U3			56.3/56.3	0/3.35	–/19
U4			53.5/53.5	0/1.89	–/18
U5			38.6/28.3	0/1.89	–/18
V1	400, 100, 100	1/2*L*	2.9/4.5	0/4.90	–/17
V2			2.1/3.3	1.89/3.35	42/13
V3	400, 100, 200	1/2*L*	4.6/4.6	1.89/1.89	42/13
V5	600, 100, 100	1/3*L*	4.0/4.0	1.89/1.89	42/15
V6	1000, 330, 100	1/4*L*	25.5/25.5	3.35/1.89	57/18
V9	400, 100, 100	1/3*L*	36.6/36.6	1.89/3.35	22/16
G1	809, 413, 110 Asymmetric	1/6*L*	25.0/25.0	3.35/3.35	24/24

Table 2
Values of ultimate load

Case	Description span, rise, width (cm)	Experimental (kN)	FEM with PROSHELL (kN)	Plastic analysis [6] (kN)	Present method (kN)
U1	400, 100, 100	19.5	–	17.96	20.0
U2	”	21.0	–	17.96	20.0
U3	”	26.0	*LG* 27.5 *NLG* 26.0	21.00	21.4
U4	”	15.2	–	11.97	10.4
U5	”	14.2	–	11.27	10.3
V1	400, 100, 100	16.3	16.5	–	16.2
V2	”	15.1	16.3		17.3
V3	400, 100, 200	21.6	24.0	–	22.0
V5	600, 100, 100	8.5	7.7		9.0
V6	1000, 330, 100	14.7	*LG-H* 12.7 *LG-C* 20.7 *NLG-C* 18.9	–	$-H$ 10.6 $-C$ 15.8
V9	400, 100, 100	45.2	45.4	–	43.5
G1	Unsymmetrical	–	14.8	–	14.0

NLG: non-linear geometric analysis; *LG*: linear geometric analysis; $-H$: hinged; $-C$: clamped.

obtained showing large residual capacity after the peak load. As predicted by the numerical analysis and confirmed by the experiments, the ultimate peak loads (Table 2) vary almost proportionally with the reinforcement; for cases U2–U5 and V9, geometrically equal and subject to the same load condition, a similar value (8000 ± 500 kN) is always obtained by dividing the ultimate load by the total (top plus bottom) reinforcement ratio.

4.2. Numerical modeling

As mentioned in Section 1, the experimental program permitted the validation of a sophisticated numerical model (PRO-SHELL) specifically developed for non-linear analysis of reinforced masonry vaults. The model is based on the micro-modeling approach, meaning that the three material components existing in the structure – the ceramic bricks, the

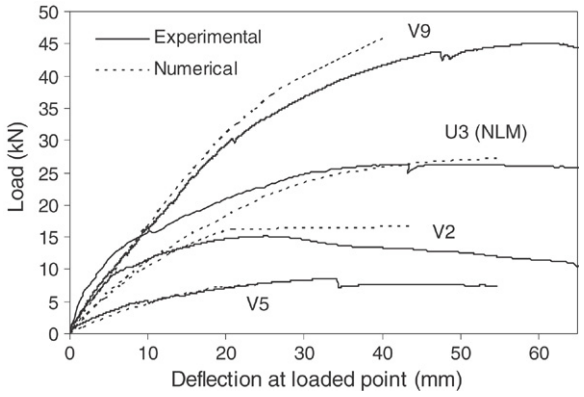

Fig. 10. Load versus vertical deflection experimental and numerical diagrams for vaults U3, V2, V5 and V9.

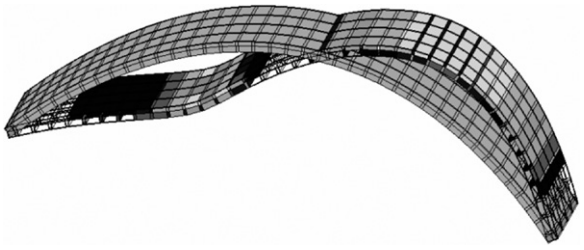

Fig. 11. Initial and deformed FE mesh at failure (×6) for vault U3.

mortar volumes and the steel rebars – are actually described as distinct components with specific constitutive equations. In fact, in a general micro-model, the unit-joint interfaces should be simulated by means of frictional joint elements, or similar devices, allowing sliding or rotation between units. To limit the required calculation effort, the hypothesis of perfect bonding between units and mortar is adopted for the present application.

Bricks and mortar volumes are described by means of solid Serendipit 3-D, 20 node elements. Using a single finite element of this type to describe each individual brick, or each portion of mortar joint between brick faces, has been demonstrated to produce adequate results. This simple treatment is made possible thanks to the capacity of the adopted element to simulate intense stress gradients across its thickness. Fig. 11 shows a typical mesh of a vault and the corresponding deformed shape at the ultimate condition for a concentrated load applied at one-quarter of the span.

The steel reinforcement is modeled as an equivalent horizontal layer referred to a solid element (brick or mortar volume) whose centre of gravity is located at the height of the actual reinforcing bar. In turn, the steel layers may be unidirectional or bidirectional to account for one or two families of parallel rebars placed approximately at the same depth.

Non-linear behavior is accounted for by a local multiaxial (isotropic) damage model for mortar and bricks and by a uniaxial elastic–plastic model for steel accounting for plastic hardening. Damage index ranges between 0 (no damage, integer status) and 1 (full damage). To describe the structural constitutive behavior of the materials (bricks, mortar, concrete and steel) the most relevant required parameters are: deformation modulus (E), Poisson's ratio (υ), tensile strength (f_t), compressive strength (f_c), plastic strain hardening ratio (H), ultimate strain (ε_f) and fracture energy (E_c). More information can be found in [10].

The model produced acceptable predictions of the ultimate load and the stress–strain diagrams (Fig. 10 and Table 2).

4.3. Comparison with the proposed method

The results obtained from the experimental and numerical studies presented in Sections 4.1 and 4.2 have been utilized to validate the method herein presented. For these calculations, the characteristic value of the compression strength of the bottom masonry f_c is calculated by means of Eq. (16), provided by Eurocode 6, using the compression strength values of mortar f_m and brick f_b,

$$f_c = K f_b^{0.65} f_m^{0.25} \tag{16}$$

where the constant K is taken equal to 0.4 in the case of hollow bricks. It is noted that Eq. (16) provides only an estimate and that further research would be needed for a more accurate prediction of the compression strength of the masonry used to build the reinforced vaults here discussed.

Table 2 compares the experimental and numerical results available with those obtained using the present method. The results obtained analytically by Lourenço et al. [6] are also considered.

The calculations carried out using PRO-SHELL always considered non-linear geometric effects, except when indicated in Table 2. Given the uncertainty in the actual behavior of the supports, experimental case V6 is computed assuming either clamped or hinged ends. Fig. 12 shows the thrust line solution (represented in "normal" mode) obtained for vaults V5 and G1.

As can be seen in the table, the estimation obtained for the ultimate load is acceptable for most of the considered cases. A slight, but acceptable, overestimation of the ultimate load is observed in some vaults built with poor mortar (cases V1, V2, V3 and V5, with f_m between 3 and 5 MPa). Conversely, the ultimate load is underestimated in the cases built with medium to high strength mortar (cases U1–U5 and V9, with f_m above 10 MPa). Among the effects which may contribute to these disagreements are (1) the inaccuracy of Eq. (16) in estimating the true compressive strength of masonry, (2) the influence of the tensile strength of the mortar, particularly in the case of high strength, and (3) the true ultimate stress of steel above the yielding limit, which is not considered in the calculations. The fact that bonding between mortar and steel may be partially lost at the ultimate condition may also affect the estimation. In spite of these considerations, the encountered errors range between 1% and 15% for most of the cases, with the exception of vaults U4 and U5, for which the error is about 30%. The slight disagreements with Lourenço et al. [6] are due to a different estimation of the compressive strength of the material and the plastic moments at the critical sections.

The estimation provided by the proposed method agrees well with other analytical solutions, such as those provided by Lourenço et al. [6] (cases U1–U5) and those calculated by means of PRO-SHELL (cases V1–V9). In particular, the

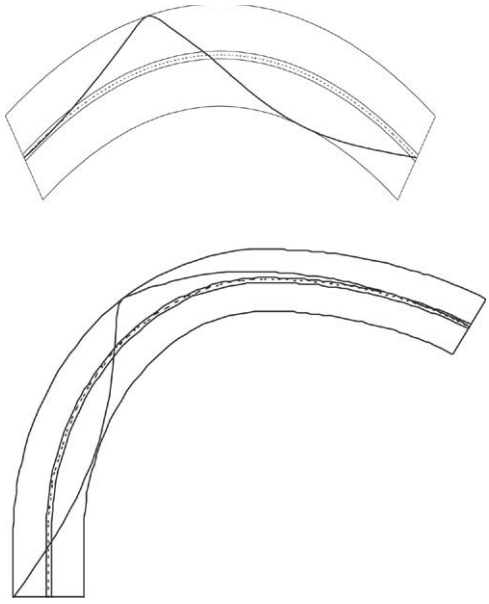

Fig. 12. Resulting thrust line solutions for vault V5 and G1 (*normal* mode).

accuracy of this method at estimating the ultimate load can be compared to that of the more complex numerical approach.

Example G1 consists of a more complex shaped, asymmetric vault spanning 8.09 m, with rise of 4.13 m, composed of a vertical segment 1.00 m high, an elliptic segment defined by a horizontal semiaxis of 3.04 m and a vertical semiaxis of 4.13 m, starting at 0° and reaching the highest point at 90°, and another elliptical segment with horizontal semiaxis of 5.05 m and horizontal semiaxis of 3.04 m, starting at 90° and ending at 125°. The material properties and reinforcement are given in Table 1. In spite of the complexity of the shape, the present method also provides an ultimate load in agreement with PRO-SHELL, with an error of only 6.5% at the safe side.

The influence of second-order equilibrium effects on the ultimate load was investigated by carrying out a non-linear geometric analysis (NLG) by means of PRO-SHELL on two selected cases corresponding to a short-span vault (U3), and a medium-span one (V6). The consideration of the second-order equilibrium effects produced a reduction of the ultimate load of 5.5% and 8.6% for the short- and medium-span vaults respectively. These results show that such effects have a small influence, although perceptible, on the response of the vaults.

5. Conclusions

A simplified method for the ultimate analysis of reinforced brick masonry arches or cylindrical shells, also usable for the analysis of reinforced concrete or plain masonry or concrete arches, is presented. The method is based on conventional plastic analysis of unreinforced masonry arches. A procedure, based on a graphical treatment of the problem, has been developed to extend this approach to the case of reinforced masonry arches and cylindrical vaults with arbitrary geometry in the longitudinal direction. The method is complemented with automatic algorithms for the application of the safe (or lower-bound) and uniqueness plasticity theorems.

The method has shown its capacity to provide engineering estimations of the ultimate loading capacity of such structures. An acceptable agreement has been attained with results obtained both experimentally and numerically, by means of a more sophisticated approach, on vaults covering a variety of situations with regards to the properties of the materials and the amount of reinforcement.

Acknowledgements

This work has received financial support from the Autonomous Catalonian Government (CIDEM, “CERARMAT” IT – Technological Innovation – project 605) the Spanish Government (Ministry of Industry and Energy, “PRECERAM” ATYCA project M172/1999) and the European Commission (“ISO-BRICK” CRAFT – Cooperative Research – Project G5ST-CT-2001-50095). All this support is gratefully acknowledged.

References

[1] Diel KL. Reinforced brick shells for large-span roofs. Ziegelindustrie International 1991;44(9):482–6.
[2] van Dijk A. The brick vaults of Eladio Dieste. Eindhoven: Eindhoven University of Technology, Faculty of Architecture, Department of Structural Engineers; 1993.
[3] CRAFT 1999-70420 Research Project ISO-BRICK, European Commission. Report about the Proposed technologies. Deliverable n. 37 (Non-confidential). 2004.
[4] Heyman J. The stone skeleton. International Journal of Solids and Structures 1966;2:270–9.
[5] Heyman J. The masonry arch. Chichester: Ellis Horwood; 1982.
[6] Lourenço PB, Palacio K, Barros J. Design recommendations for reinforced masonry arches. In: Arch Bridges VI. Barcelona: International Center for Numerical Methods in Engineering (CIMNE); 2004. p. 583–92.
[7] CEN. Eurocode 6: Design of masonry structures. ENV 1996-1-1:1995. Brussels: CEN; 1995.
[8] Andreu A, Gil L, Roca P. Limit analysis of masonry structures by simulation of the equilibrium of funicular systems. In: Métodos Computacionais em Engenharia. Lisboa: LNEC; 2004. p. 83 [in Spanish].
[9] Sarrablo V. Contribution to the viability of laminar reinforced masonry roofs using semi-prefabricated solutions. Proposal for short span cylindrical shells. Ph.D. dissertation. Barcelona: Universitat Politècnica de Catalunya; 2002 [in Spanish].
[10] Hanganu AD, Oñate E, Barbat AH. A finite element methodology for local/global damage evaluation in civil engineering structures. Computers and Structures 2002;80:1667–87.